Advances in Bridge Engineering

ORIGINAL INNOVATION

Open Access

Comprehensive index condition assessment of structural concrete based on surface wave techniques

Xiang Xu[1*], Jiasheng Lan[2], Ahmet Serhan Kırlangıç[3] and Maria Anna Polak[4]

*Correspondence:
xxuseu@126.com

[1] School of Transportation, Southeast University, Nanjing, China
[2] International Education School, Suzhou University of Science and Technology, Suzhou, China
[3] Civil Engineering, Bahcesehir University, Istanbul, Turkey
[4] Civil and Environmental Engineering, University of Waterloo, Waterloo, Canada

Abstract

To reliably assess the condition of concrete structures, a surface wave-based comprehensive index has been developed. Considering various factors (e.g., aggregate types) influencing the surface wave-based characteristics, a relative index for concrete condition assessment has presented. To address the conflicts between individual indexes, the weight for each index is determined in accordance with its credibility. The effectiveness of the proposed methodology is verified by using test results from six concrete beams with different void volume ratios. Hereby three characteristics of surface waves (i.e., P- and R-wave velocities, and attenuation coefficient) are used to diagnose the concrete beams. It is found that the comprehensive index has the advantage in handling abnormal measurements of the individual indexes by reducing their weights to lower their influence on the final diagnosis. Comparison of the diagnoses based on the comprehensive index and individual indexes reveals that the comprehensive index performs much better than any other individual index. It matches greatly with the compressive strength of the concrete beams obtained from the destructive test. In conclusion, the proposed methodology presents a single comprehensive diagnostic feature with improved reliability on the fitness of the concrete structures for decision-makers.

Keywords: Non-destructive testing, Damage assessment, Concrete beams, Data analysis, Risk management

1 Introduction

Non-destructive testing (NDT) techniques have been widely used for inspection and evaluation of civil engineering structures due to their capability in detecting hidden defects (Lim & Cao, 2013). In the last decades, beneficial NDT methods have been developed for determination of properties of concrete (McCann and Forde 2001). The most common techniques in the industry are: (1) acoustic emission, which is used to detect, locate and characterize damages in concrete based on the fact that irreversible changes in the internal structure are accompanied by radiation of acoustic waves (Ohtsu

1996); (2) ground penetrating radar, which is effective for subsurface concrete assessment on the basis that electromagnetic waves sent by radars refract and reflect when they encounter different materials (Belli et al. 2008); (3) infrared thermography, which is usually applied to locate the void, delamination and other defects in concrete on the foundation that heat flows more slowly through defects (air) than through solid concrete (Cheng et al. 2008); and 4) ultrasonic testing, which uses ultrasonic pulse-waves transmitting into materials to detect internal flaws or characterize materials.

Ultrasonic tests are well-established and widely used because of their fast execution, low cost and practicability (Ihara 2008). Currently, a wide range of sensors, instruments and sophisticated software are available for ultrasonic testing. The most common ultrasonic tests available in the commercial market include ultrasonic pulse velocity (UPV), impact echo (IE) and spectral analysis of surface waves (SASW). The UPV test uses a pulse travelling through the concrete to evaluate its elastic properties and density based on the measured compressional wave velocity (Karaiskos et al. 2015). The IE technique is capable of locating defects in the form of void and delamination or measuring element thickness by means of monitoring the arrival of the stress waves (Hsieh et al. 2017). The SASW method is used to obtain the dispersion of surface waves from which the shear modulus and thickness of the layers in concrete are determined (Cho 2003). The traditional SASW incorporates two receivers, therefore, the repetitions of the test is required for different source-receiver spacing in order to investigate the medium at different depths. To reduce the repetitions, the multi-channel analysis of surface waves (MASW) testing, which was originally developed for estimating the shear profile of the soils (Park et al. 1999), is adopted for the concrete materials as an ultrasonic test (Yang et al. 2009; Kirlangic, Cascante, & Polak, 2016). The MASW test configuration includes equally spaced multiple receivers, of which the data obtained are used to evaluate the overall condition of structural elements.

Characteristics of surface waves (e.g., group and phase velocities, and attenuation coefficient), which can be determined from the MASW tests, provide information on the condition of material and thus can be used as diagnostic indexes for condition assessment of concrete. Besides the damage condition of material, many other factors also affect these characteristics, including aggregate types and cement-water ratio (Kewalramani & Gupta, 2006). Therefore, it is difficult to define an absolute assessment criterion based on the wave characteristics for different types of concrete members. Given the various influencing factors, the characteristics should be interpreted in a relative manner instead of being used to evaluate condition of concrete directly (Rodriguez Roblero 2017).

Although many surface wave-based methodologies for condition assessment of concrete have been established, each methodology represents the condition of concrete in its own way and its reliability does not only rely on the nature of the feature investigated also on the errors in the test procedure. As a result, conflicts inevitably exist between the diagnoses performed based on the indexes derived from different methodologies. Such conflicting diagnoses may mislead the decision for structural maintenance. Hence, developing a combination methodology of individual diagnostic indexes is at the foremost importance for improving the reliability of the diagnosis.

In this study, a comprehensive diagnostic index for condition assessment of concrete is proposed based on the material properties extracted from the surface waves, namely P- and R-wave velocities, attenuation coefficient, and material damping ratio. First, the properties are estimated by processing the ultrasonic signals acquired by the MASW tests, and then a relative index form is built to evaluate the condition of the concrete. The methodology aggregates the individual indexes into a comprehensive one based on the similarities between these indexes. This fusion procedure is demonstrated based on multiple diagnostic features obtained from the ultrasonic test conducted on six laboratory scale beams with different void volume ratios (Kirlangic et al., 2016). The comprehensive index addresses the conflicts between diagnoses based on multiple indexes and helps owners make maintenance decisions in a straightforward and reliable manner.

2 Experimental investigation

2.1 Cast of concrete beams

Six beams (Fig. 1) of dimensions $110 \times 15 \times 10$ cm, containing different void volumes, are produced and tested as described by Kirlangic et al. (2016). Voids are created by mixing the concrete with Styrofoam pellets of 7 mm diameter. Beam 1 is the control beam with 0% artificial void in volume (i.e., no added pellets), whereas the other beams have 5%, 10%, 15%, 20% and 30% void volume (denoted by ϕ), respectively. After curing period, all the beams are moved to the laboratory environment and kept under normal conditions until all the ultrasonic and mechanical tests are completed.

2.2 Mechanical tests

The compressive strengths of the concrete beams are measured in accordance with CSA A23.2-9 C for both rectangular prisms cut out from the beams and concrete cylinders, which are produced at the time of casting. The average compressive strengths of the

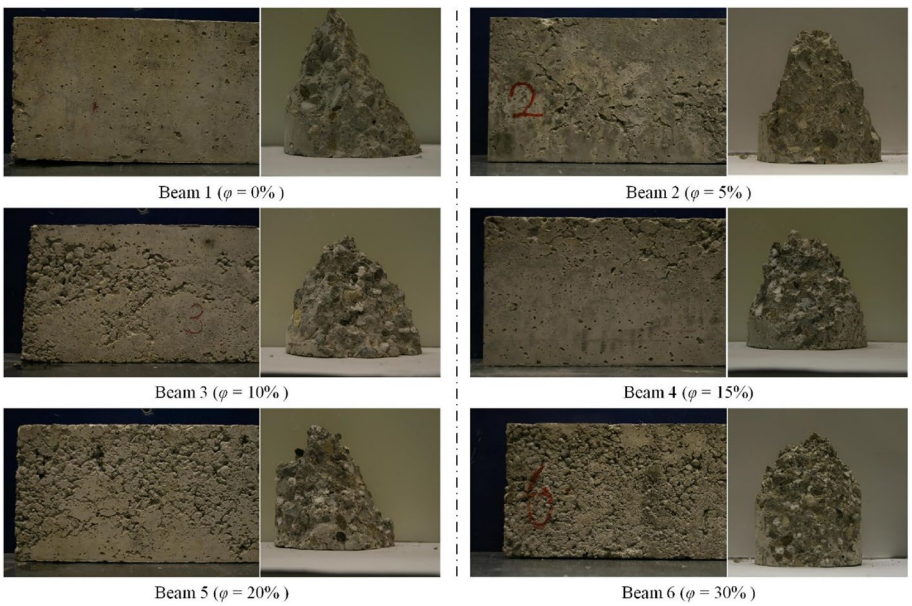

Fig. 1 Six beams and their associated cylinder samples

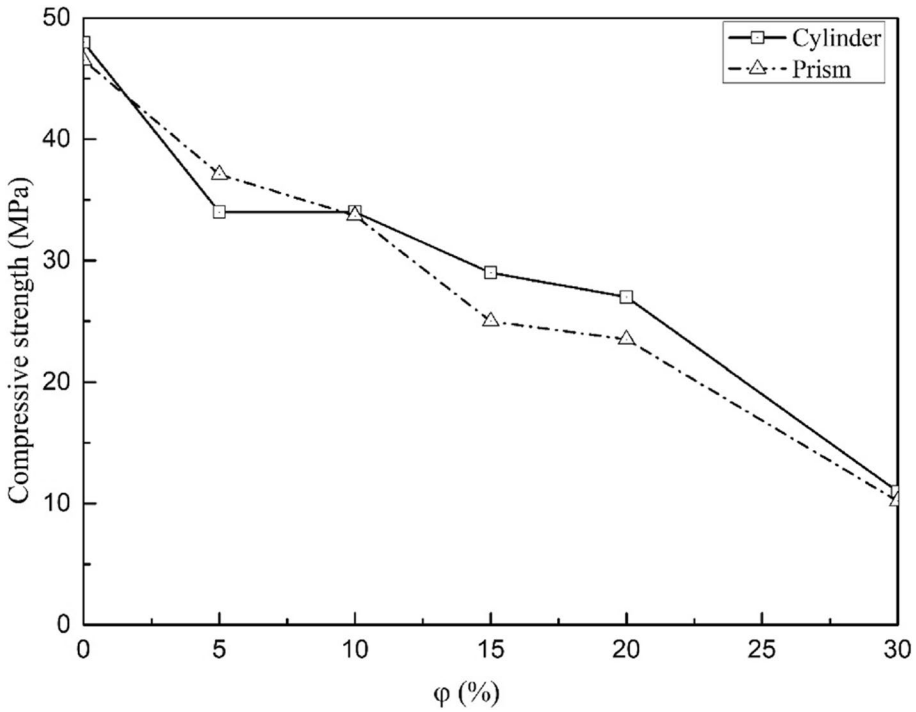

Fig. 2 Compressive strength for cylinders and rectangular prisms

specimens are shown in Fig. 2. The strengths of both cylinders and prisms exhibit similar trends, which drop from 50 MPa to 10 MPa with increasing void ratio. The initial 5% void causes approximately a 20% drop in strength, while both 15% and 20% void volumes reveal the same level of strength. This can be attributed to the fact that the real void volume does not differ meaningfully between the investigated sections of these two beams.

2.3 Ultrasonic tests

The instrumentation used for the ultrasonic tests (Fig. 3) consists of a piezoelectric transmitter (50 kHz resonant frequency) which is driven by a pulse, 18 accelerometers (Dytran 3055B3, 35 kHz resonant frequency, 1 Hz − 10 kHz flat response, 504.1 mV/g

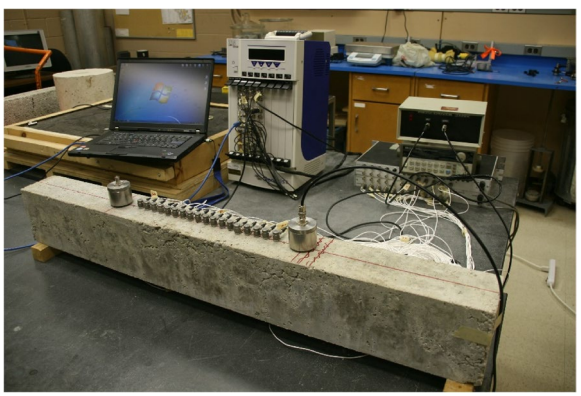

Fig. 3 Ultrasonic test instrumentation

sensitivity) as receivers, two external power supplies (PCB 483 A) to run all of the accelerometers at once, and a data acquisition system (Genesis, 24 channel, 1 MHz sampling rate) to capture the wave signals (Kirlangic et al., 2016). A built-in 100 kHz low-pass Bessel filter, which is available within the acquisition unit, is used during the signal acquisition. All the receivers are fixed at once along the centre line of the beams through nuts; a commercial glue is used as coupling between the beams and nuts. The total length of the receiver array is 40 cm with a receiver spacing of 2 cm. In addition to the vertical placement of the transmitter on the beams, the source is also mounted horizontally on the edge of the beam to excite the longitudinal waves. The transmitter is supported with a ratchet strap in this position where vacuum grease is used as coupling.

3 Analytical investigation

3.1 Characteristics of surface waves

The recorded signals from the MASW testing are investigated to extract the material characteristics, namely P-wave velocity (V_P), R-wave velocity (V_R), attenuation coefficient (α) and material damping ratio (D) as described below.

3.1.1 Primary and Rayleigh wave velocities

In an unbounded medium, two types of waves are observed: dilatational (compressional) and distortional (shear) waves. Particle motion is along the direction of the wave propagation in the compressional waves, whereas the particles move perpendicularly to the propagation in the shear waves. The velocity of compressional wave, commonly known as P-wave velocity, is related to the Young's modulus E, Poisson's ratio ν, and mass density ρ as given by (Rodriguez Roblero 2017)

$$V_P = \sqrt{\frac{E(1-\nu)}{\rho(1+\nu)(1-2\nu)}} \tag{1}$$

Equation (1) describes the velocity of the dilatation in a homogenous medium. On the other hand, the shear-wave (S-wave) velocity in an unbounded homogenous medium is expressed by

$$V_S = \sqrt{\frac{G}{\rho}} \tag{2}$$

where G is the shear modulus of the material.

P- and S-waves are called body waves since they occur in infinite medium. In the case of only one traction-free boundary, the body waves interact with each other along the free surface and generate the surface waves, also known as Rayleigh waves. The velocity of the surface waves V_R is governed by the following Rayleigh-frequency Eq.

$$\left[2-\left(\frac{V_R}{V_S}\right)^2\right]^4 = 16\left[1-\left(\frac{V_R}{V_P}\right)^2\right]\left[1-\left(\frac{V_R}{V_P}\right)^2\right] \tag{3}$$

Equation (3) implies that the Rayleigh wave (R-wave) velocity V_R depends on the body wave velocities V_P and V_S, which means that V_R only relies on the properties of the material. Hence, the R-waves propagate in a non-dispersive way, in other words, waves with any wave-length in the propagation travel at the same velocity.

Wave propagation in a bounded medium is more complicated compared to a semi-infinite medium due to multiple reflections of waves between the boundary surfaces and mode conversions of body waves. In the case of a plate, the interaction of waves generates Lamb modes as defined with the Rayleigh-Lamb frequency equation (Graff 1975)

$$\frac{\tan(\beta d)}{\tan(\alpha d)} + \left[\frac{4\alpha\beta\kappa^2}{(\kappa^2-\beta^2)^2}\right]^{\pm 1}, \begin{cases} +1 = symmetrical \\ -1 = antisymmetrical \end{cases} \tag{4}$$

where $\alpha^2=\kappa^2-\omega^2/V_P^2$ and $\beta^2=\kappa^2-\omega^2/V_S^2$. The variables κ, ω and d are the wave-number, angular frequency and medium thickness, respectively. The Lamb modes are frequency-dependent (in other words, dispersive). However, at high frequencies they are considered Rayleigh waves travelling at constant velocity because the wavelengths are shorter than the medium thickness.

The velocities of body and surface waves can be estimated from the time histories of the signals obtained from the multi-channel tests. Hereby, the P- and R-wave velocities are calculated by an algorithm, which detects the arrival time of these two waves at different distances in an automated way (Kirlangic et al., 2016). Then, linear regression is performed on these selected points on the time-offset plot in order to estimate the velocities which are basically the slope of the fitted lines. P-wave velocity is determined by using the pseudo-colour plots generated by MATLAB as shown in Fig. 4 (a). An automated code, developed in MATLAB, is used to calculate the R-wave velocity, in which the same threshold value of amplitude is defined for all time histories in order to pick the normalized peak-to-peak amplitudes and their corresponding arrival times. The normalized peak-to-peak amplitudes are to make travelling distance of each wave the same. In the code, prior to the velocity computation, the arrival of the wave-front is extracted by using a time window in order to select the first arriving peak of the surface wave. Typical R-wave fronts for concrete are presented in Fig. 4 (b) on a generic time-offset plot which is obtained from a multi-channel testing.

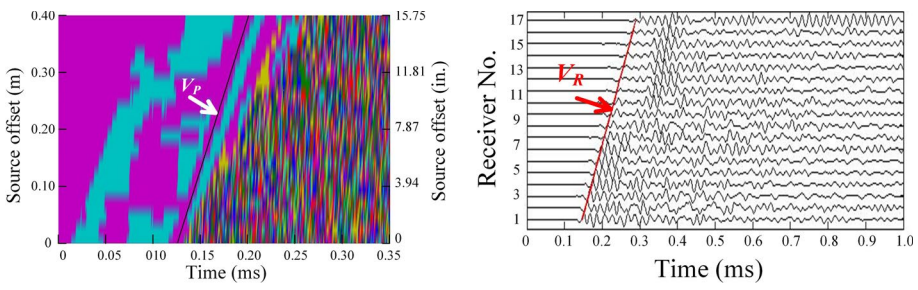

(a) Pseudo-color plot for calculation of V_P (b) Time-offset plot for calculation of V_R

Fig. 4 Typical estimation methods of VP and VR from multi-channel testing

P-wave velocity (V_P) is correlated to the compressive strength of concrete (S) and the most commonly accepted correlation relationship is $S = a\exp(bV_P)$, where a and b are empirical parameters determined by means of regression analysis (Trtnik, Kavcic, & Turk, 2009). While R-wave velocity is exploited to estimate porosity in concrete by investigating its relationship with the porosity in dry and fully saturated mortars (Goueygou et al. 2009). Thus, both the P- and R-wave velocities are acceptable as the indexes demonstrating the condition of concrete.

3.1.2 Attenuation and material damping ratio

Energy dissipation of waves is caused by geometric radiation and deformation. The former is related to increasing surface area of the propagating wave-front and the latter represents the material damping. The total attenuation of a propagating wave is defined as (Graff 1975)

$$\frac{A_1}{A_2} = \left(\frac{x_1}{x_2}\right)^{\beta} e^{\alpha_x(x_1 - x_2)} \tag{5}$$

where A_1 and A_2 are the amplitudes at distances x_1 and x_2 from the source, β is the geometric attenuation constant, which is assumed as -0.5 for surface waves (cylindrical wave fronts) (Zerwer, 2002), and α_x is the spatial coefficient of wave attenuation which is related to the material damping. Rearranging Eq. (5) gives:

$$\alpha_x = \frac{1}{x_2 - x_1}\left[\ln\left(\frac{A_1}{A_2}\right) - \beta \ln\left(\frac{x_2}{x_1}\right)\right] \tag{6}$$

The relation between α_x and the material damping ratio (D) is given as a function of frequency (Zerwer, 2002):

$$D = V\frac{\alpha_x}{\omega} \tag{7}$$

where V is the wave velocity, in this case it is the velocity of Rayleigh wave and ω is the angular frequency.

When an ultrasonic wave propagates through a medium, the attenuation due to the loss of energy is observed as a reduction of amplitude of the wave. Some of the factors affecting the amplitude, and the waveform of the ultrasonic waves are ultrasonic beam spreading, energy absorption, dispersion etc. In general, the higher frequencies (i.e., shorter wave-lengths) attenuate more rapidly compared to the lower frequencies, thus the attenuation coefficient highly depends on frequency. Since this frequency dependence reflects the structures of materials in different levels, it can be used for characterizing the material properties at both micro and macro scales relating to chemical reactions and mechanical processes. Besides, compared to P- and R-wave velocities, attenuation is more sensitive to the damages in concrete materials (Kirlangic 2013).

Determination of the total attenuation coefficient α can be performed based on wave characteristics either in time or frequency domain by using a variety of signal processing techniques. Hereby, the discrete wavelet transform (DWT) based on Mallat's algorithm (Mallat 1989) is adopted to process the signals obtained from MASW tests for extracting the coefficient α. The DWT algorithm provides a general picture of the

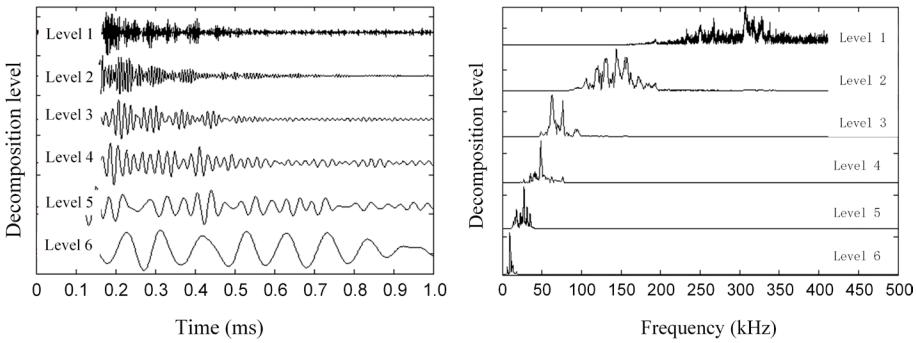

(a) Normalized decomposed time signals (b) Normalized Fourier spectra

Fig. 5 Typical decomposed signals and the associated frequency spectra

frequency distribution of a signal over time that cannot be given by the Fourier transform. It decomposes a signal into several components and each component is called a level carrying a specific frequency band-width. For demonstration, an original signal and its levels decomposed by using a Daubechies wavelet (dbn18) are shown in Fig. 5 (a), where only six levels carrying the most of the energy are displayed. Each signal's Fourier spectrum is also provided in Fig. 5 (b). Then, the level which overlaps significantly with the bandwidth of the transmitter used in the tests is selected to indicate the attenuation trends based on the spectral area. The attenuation trends are fitted to $e^{\alpha(x_1-x_i)}$ to estimate the total attenuation coefficient α, in which x_i is the location of the receiver with respect to the source. As an example, the measured and curve-fitted total attenuation trends are shown in Fig. 6, in which the total attenuation coefficient α is estimated as 2.2.

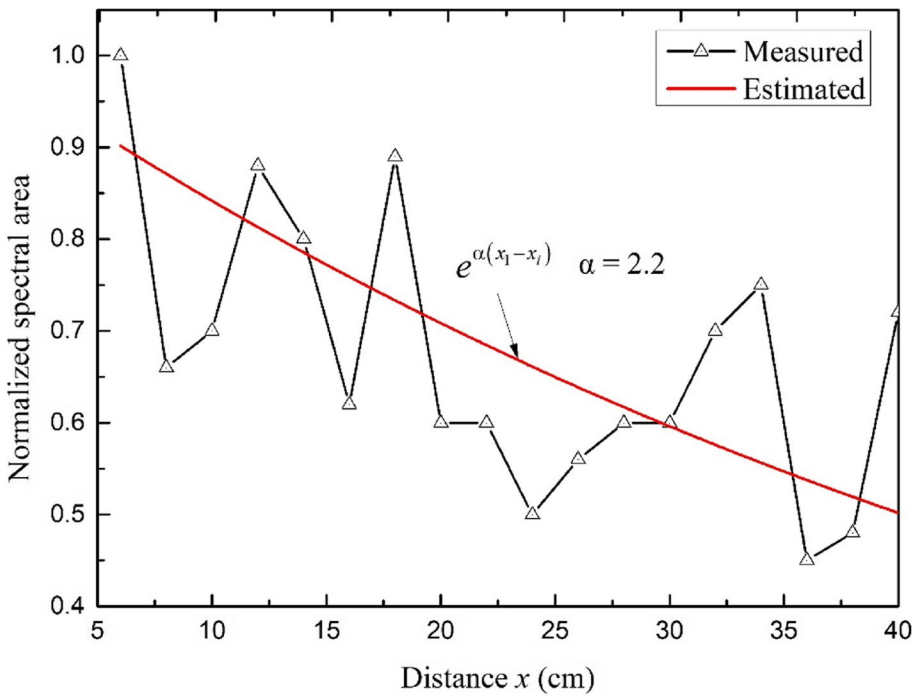

Fig. 6 Measured and curve-fitted attenuation trends

In order to determine the material damping ratio, the geometric attenuation must be eliminated from the total attenuation. Even if the reflections could be eliminated by applying a window, a geometric attenuation coefficient of -0.5 does not fit beam geometry, and thus, the computed material damping ratio could not capture the damage level. Therefore, the damping ratio is not adopted to evaluate the condition of the concrete beams in this study.

3.2 Evaluation index in a relative sense

The measured values of the aforementioned characteristics of surface waves are not only related to the material properties, such as elastic modulus and density, also the other physical conditions (i.e., damage and aging). Other than these parameters, the measurements are also influenced by test instrumentation and operator's experience. For example, P-wave velocity is affected by various factors (Blitz and Simpson 1995), specifically, deterioration in the material may cause variation as large as 20% (ASTM, 2002), and the age of concrete may result in V_P increasing by about 40% in the early three years (Popovics 2001). On the other hand, the UPV test, which is conducted to measure the P-wave velocity, is reported to have low within-test variation. ACI 228.1R-03 (2003) compares the within-test coefficient of variation (COV) reported by several researchers and gives the maximum COV as 1.9% which is consistent with 2% error in test repeatability for different operators using the same instrument (or one operator using different instruments) according to ASTM C597-16. Therefore, formulation of a relative evaluation index has significant importance owing to the challenges in assessing condition of concrete structures by using absolute values of the measured characteristics.

A normalized relative index *RI* is defined as the percentage of the wave characteristic (diagnostic feature) from the damaged concrete to the intact one:

$$RI = \frac{C - C_0}{C_1 - C_0} \times 100\% \tag{8}$$

in which C is the measured value of the characteristic, C_0 is the measured value ofor the unacceptable condition of concrete, and C_1 is the one for the intact condition of concrete. For P-wave velocity, Saint-Pierre, Philibert, Girous, and Rivard (2016) defined $C_0 = 1500$ m/s (which is the velocity of primary waves through water), and C_1 the measured value on intact concrete specimen in the lab.

When the measured value C approaches C_1, the indicator *RI* tends toward 100% which indicates that the concrete is in its intact condition; while a value close to C_0 leads *RI* to 0% which corresponds to the unacceptable condition for concrete. Thus, the defined indicator *RI* has a clear physical meaning that it represents a variation ranging from the intact condition of material (100%) to the unacceptable condition (0%).

3.3 Combination methodology for individual indexes

Each surface wave-based index describes the condition of material in its own way, thus it is impractical for decision makers to make decisions for maintenance via multiple diagnostic indexes, especially in the case of conflicts among them. Moreover, each single characteristic will have its own limitations in condition assessment of material; while a comprehensive index derived from multiple characteristics can conduct a more

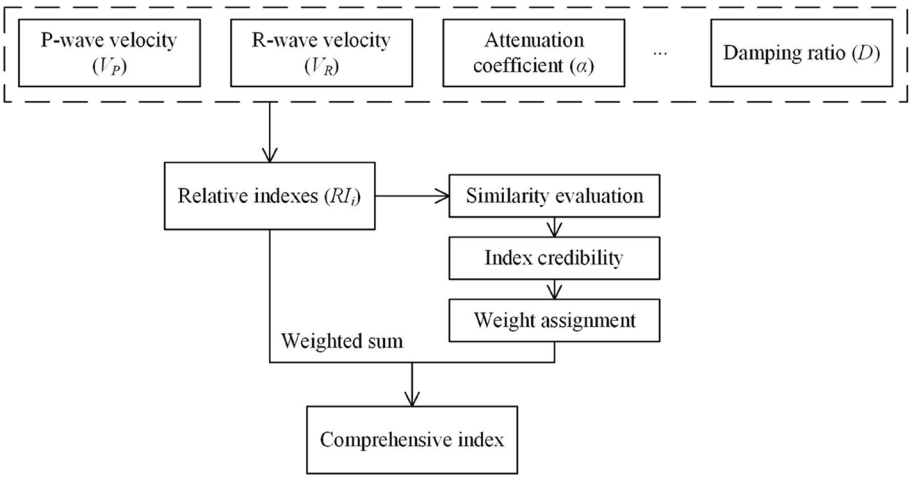

Fig. 7 Procedure for the calculation of the comprehensive index

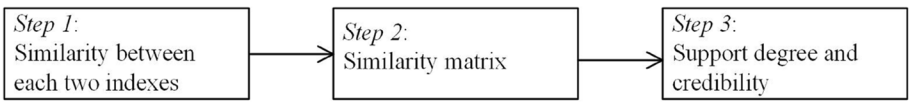

Fig. 8 Steps to determine the index credibility

robust diagnosis because multiple diagnoses information can support each other. Therefore, combining the individual indexes into a comprehensive one is not only convenient for decision makings, but also increases the reliability of the assessment results by data fusion procedure.

Weighted sum is the most common approach for the combination of multiple diagnostic indexes, where the key point is to allocate a weight to each index rationally. Based on the assumption that the majority of the diagnostic indexes (in this case, the surface wave features) are credible, an index that is conflicting with the others should contribute less to the final comprehensive index, in other word, such index deserves smaller weight value. The weights of the indexes are assigned based on the credibility of the index, which is evaluated by similarities between the indexes. The procedure for the calculation of the comprehensive index is illustrated in Fig. 7.

3.3.1 Determination of the index credibility

The weight of each individual index is allocated based on its credibility that is determined by the similarities between the indexes. The steps for determination of the index credibility are shown in Fig. 8.

3.4 Step 1: similarity between each two indexes

First, the similarity between each two indexes is estimated using the cubic of cosine similarity that is a measure of similarity between two non-zero vectors of an inner product space that measures the cosine of the angle between them (Sidorov et al. 2014). The

vector is constituted of *RI* and (1 - *RI*), where *RI* is the normalized relative index. Two vectors with the same orientation have a cosine similarity of 1 that means the two vectors are identical; while two vectors diametrically opposed have a similarity of -1. The similarity degree (sim_{ij}) between two indexes *i* and *j* can be expressed as

$$sim_{ij} = \left[\frac{\mathbf{RI_i} \cdot \mathbf{RI_j^T}}{\sqrt{\left(\mathbf{RI_i} \cdot \mathbf{RI_i^T}\right)\left(\mathbf{RI_j} \cdot \mathbf{RI_j^T}\right)}} \right]^3 \tag{9}$$

where $\mathrm{RI}_i = (RI_i, 1 - RI_i)$, and RI_i is the normalized relative index *i* ($0 \leq RI_i \leq 1$). Because the element values in vector RI are both positive, two vectors significantly opposed have a similarity of 0 in this case. For instance, two evaluation results of a given concrete element are $\mathrm{RI}_1 = (1, 0)$ and $\mathrm{RI}_2 = (0, 1)$, respectively. Index 1 indicates the concrete element in intact condition while Index 2 exhibits the element in very poor condition, which are the completely conflicting diagnoses. In this case, the cosine similarity of the two vectors equals to 0.

3.5 Step 2: similarity matrix

Once the similarities between each two indexes are obtained, an N × N similarity matrix (SIM) can be built as

$$\mathrm{SIM} = \begin{bmatrix} 1 & sim_{12} & \dots & sim_{1N} \\ sim_{21} & 1 & \dots & sim_{2N} \\ \vdots & \vdots & \ddots & \dots \\ sim_{N1} & sim_{N2} & \dots & 1 \end{bmatrix} \tag{10}$$

where *N* is the number of total indexes. The similarity matrix illustrates the overall conflicting circumstance between all the indexes.

3.6 Step 3: support degree and credibility

The support degree is used to measure the conflicts between the target index and the other indexes. If the target index is similar to the majority of other indexes, namely, most other indexes support the target index firmly, the target index deserves a high support degree. The degree of support (Sup_i) that all the other indexes provide to the index *i* is

$$Sup_i = \sum_{j=1, j \neq i}^{N} sim_{ij} \tag{11}$$

Then, index credibility is calculated by normalizing the support degree as

$$Cred_i = \frac{Sup_i}{\max\limits_{1 \leq j \leq N} \left(Sup_j\right)} \tag{12}$$

Based on Eq. (12), the index with the maximum support degree has an index credibility of 100%.

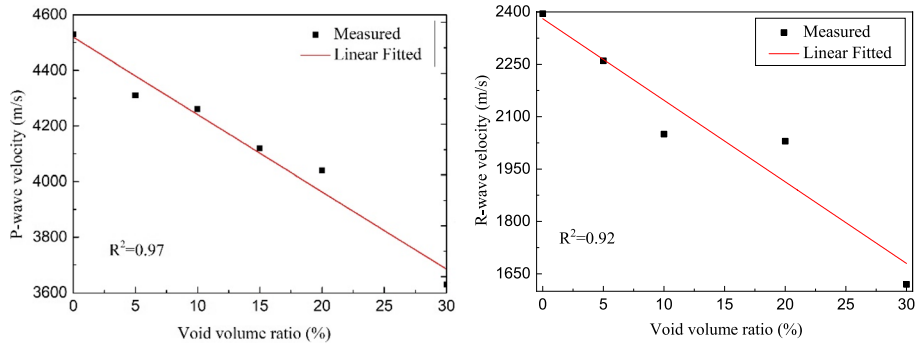

(a) Measured values of P-wave velocity (b) Measured values of R-wave velocity

Fig. 9 Measured values of P- and R-wave velocities

3.6.1 Weight assignment based on index credibility

The indexes with high credibility deserve large weights to increase the reliability of the diagnosis. Thus, the weights should be allocated in accordance with their credibility as

$$\omega_i = \frac{Cred_i^n}{\sum_{j=1}^{N} Cred_j^n} \tag{13}$$

where n is the coefficient which adjusts weight distribution with regard to the credibility. For instance, if $n=0$, an average weight is assigned to each index; while, the bigger the value of n is, the stronger the preference towards highly credible indexes.

In the final step, the weighted sum method combines the individual indexes into a comprehensive index in accordance with their weights as follows:

$$RI_{comp} = \sum_{i=1}^{N} RI_i \omega_i = \sum_{i=1}^{N} \frac{RI_i \cdot Cred_i^n}{\sum_{j=1}^{N} Cred_j^n} \tag{14}$$

4 Data analysis

4.1 Measurements from ultrasonic tests

4.1.1 P- and R-wave velocities

The trend shown in Fig. 9 (a) exhibits a negative correlation between the void ratio and P-wave velocity. It drops from 4530 to 3630 m/s in a linear fashion with a standard deviation (σ) of 305 m/s and a coefficient of variation (COV) of 7.4%. When the experimental trend is fitted into a linear line, the coefficient of determination (R^2) is found as 0.97. On the other hand, the computed R-wave velocities vary within a range of 1600 and 2400 m/s and displays a declining trend upon the void ratio with a standard deviation of 260 m/s and COV of 12.6% as shown in Fig. 9 (b). Although the R^2 is attained as high as 0.92 indicating the linear relationship, the R-wave velocity is not as sensitive to the void ratio as the P-wave velocity, especially for the beams with intermediate void ratios.

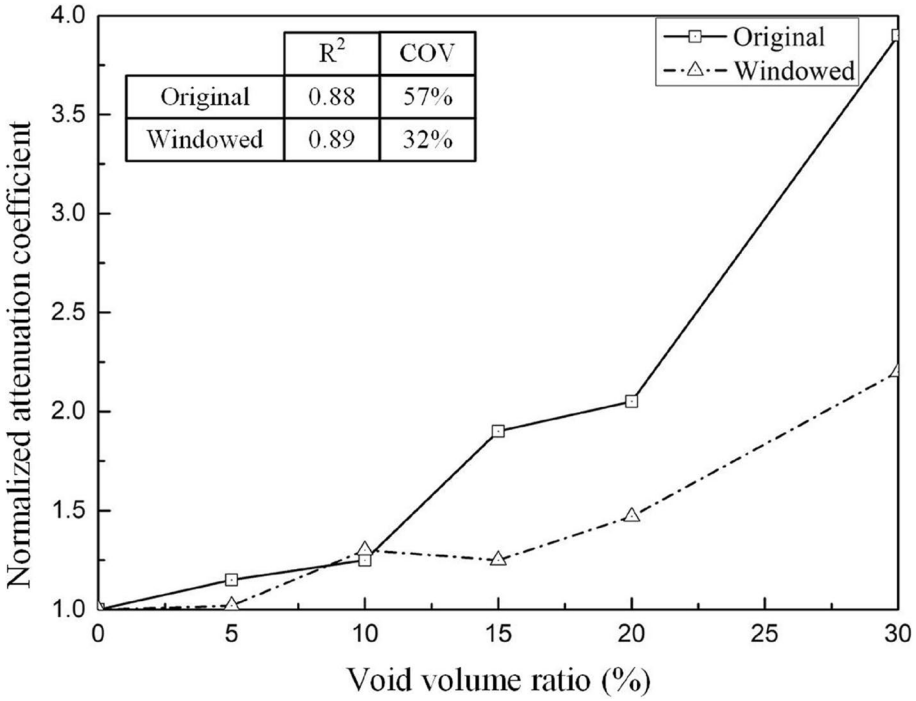

Fig. 10 Attenuation coefficients vs. void volume ratio

4.1.2 Attenuation coefficient

The total attenuation coefficient, α, is determined from the spectral area of the level 4 (bandwidth: 31-62.5 kHz) decomposed signals utilizing DWT as this bandwidth carries the most of the wave energy generated by the transmitter. The variations in α calculated from both the original and windowed sub-signals are displayed with respect to the void volume ratio in Fig. 10. For the attenuation coefficient obtained from the original signals, it is observed that α increases by a factor of 2 with respect to its initial value for a void ratio of 20%, then a large jump is apparent for 30% void ratio, making the sensitivity of α with respect to the damage level questionable. Therefore, a Tukey window is applied to signals before determining attenuation coefficient, which reduces the level of jumps observed earlier. Moreover, R^2 and COV are improved from 0.88 to 57% to 0.89 and 32% successively. It is evident that eliminating the reflections improves the results simply because the dual effect caused by the reflected waves is omitted in the attenuation calculation. For instance, in the case of Beam 1 (no void), the reflected event may be as strong as the incident event; on the other hand, in the case of Beam 6 (30% void ratio), both incident and reflected waves are attenuated faster due to large void content.

Linear correlations are observed for the compressive strength f_c', P- and R-wave velocities, and attenuation coefficient with respect to the defect amount. The statistical findings are summarized in Table 1.

In conclusion, P- and R-wave velocities, and attenuation coefficient are found as the promising characteristics for quantifying the defect volume of the concrete beams.

Table 1 Summary of the statistics for characteristics

Characteristic	Statistics			
	σ	COV	R^2	Sensitivity[a]
f_c' (MPa)	12.7	43%	0.98	79
V_P (m/s)	305	7.4%	0.97	20
V_R (m/s)	260	12.6%	0.92	32
α (m^{-1})	2.5	32%	0.89	122

[a] Sensitivity refers the total change over to the initial value

Table 2 Values of relative indexes for concrete quality evaluation

Void volume ratio (%)	Relative index		
	P-wave velocity RI 1 (%)	R-wave velocity RI 2 (%)	Attenuation coefficient RI 3 (%)
0	100.00	100.00	100.00
5	77.17	86.08	95.45
10	73.91	56.96	72.73
15	57.61	58.23	74.54
20	48.91	53.16	50.00
30	0.00	0.00	0.00

4.2 Calculation of the relative index RI

First, the values of parameters C_0 and C_1 in Eq. (8) for each characteristic are determined. In this study, the value of characteristic corresponding to the intact condition, C_1, is taken as the measured value of Beam 1 (no void); while the value of characteristic corresponding to the unacceptable condition, C_0, is the value of Beam 6 (30% void volume). As a result, the relative index values obtained from the characteristics of surface waves are listed in Table 2.

4.3 Derivation of comprehensive evaluation result

Following the steps in Fig. 8, the similarity of each two indexes is first computed using Eq. (9). For example, the similarity degree of RI_1 and RI_2 with respect to the concrete beam with void volume ratio of 5% is:

$$sim_{12} = \left[\frac{[RI_1, 1-RI_1] \cdot [RI_2, 1-RI_2]^T}{\sqrt{[RI_1, 1-RI_1] \cdot [RI_1, 1-RI_1]^T} \sqrt{[RI_2, 1-RI_2] \cdot [RI_2, 1-RI_2]^T}} \right]^3 = 97.59\%$$

The overall calculation results of the similarity degrees are listed in Table 3 according to the values of relative indexes in Table 2.

Once acquiring the similarity of each two indexes, the similarity matrix can be built. For instance, a 3×3 similarity matrix (SIM) regarding the concrete beam with 10% void volume is.

Table 3 Overall calculation results of the similarity degrees

Void volume ratio (%)	Similarity degree		
	sim_{12} (%)	sim_{23} (%)	sim_{31} (%)
0	100.00	100.00	100.00
5	97.59	98.10	91.64
10	86.55	88.12	99.94
15	99.97	87.73	86.75
20	98.92	99.40	99.92
30	100.00	100.00	100.00

Table 4 Credibility of the three indexes

Void volume ratio (%)	Index credibility		
	P-wave velocity Cred 1 (%)	R-wave velocity Cred 2 (%)	Attenuation coefficient Cred 3 (%)
0	100.00	100.00	100.00
5	90.41	100.00	91.16
10	97.53	80.13	100.00
15	98.45	100.00	80.34
20	99.28	98.49	100.00
30	100.00	100.00	100.00

$$\mathrm{SIM} = \begin{bmatrix} 100.00\% & 86.55\% & 99.94\% \\ 86.55\% & 100.00\% & 88.12\% \\ 99.94\% & 88.12\% & 100.00\% \end{bmatrix}$$

It can be seen from the above similarity matrix that RI_1 and RI_3 are extremely similar with a similarity degree of 99.94%, while RI_2 has relative large conflicts with the other two indexes corresponding to the degrees of 86.55% and 88.12%, respectively. In this case, the support degree of the three indexes are obtained based on Eq. (11), which are.

$Sup_1 = 86.55\% + 99.94\% = 186.49\%$

$Sup_2 = 86.55\% + 88.12\% = 174.67\%$

$Sup_3 = 99.94\% + 88.12\% = 188.06\%$

Then, the support degree is normalized as credibility of each index, namely,

$Cred_1 = \frac{186.49\%}{188.06\%} = 97.53\%$

$Cred_2 = \frac{174.67\%}{188.06\%} = 80.13\%$

$Cred_3 = \frac{188.06\%}{188.06\%} = 100.00\%$

The final values of the credibility of the three indexes with respect to all the six concrete beams are listed in Table 4.

The weight of each index is allocated by taking root in the credibility values in Table 4. However, the key issue here is to decide the rational value of parameter n in Eq. (13). In this paper, the value of n is optimized by making the evaluation results in line with the compressive strength. The optimization of objective function for parameter n herein is defined as

$$f(n) = \sum_{\varphi=0,5,10,15,20,30} \left(RI_{comp}^{\varphi} - RI_{cs}^{\varphi} \right)^2 \tag{15}$$

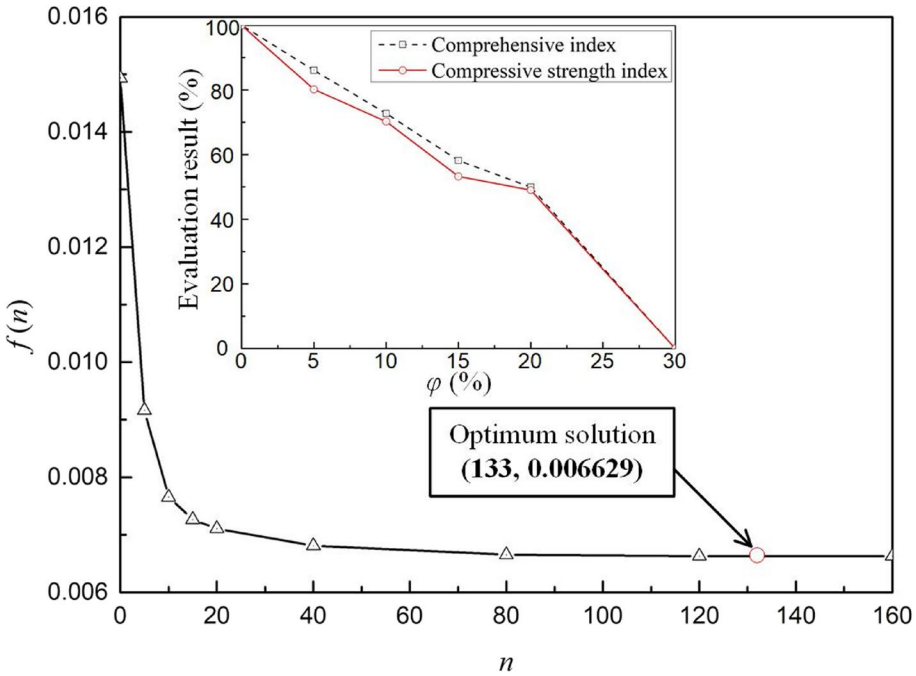

Fig. 11 Optimization process for parameter *n*

where ϕ is the void volume ratio ($\phi = 0$ refers to 0% void volume ratio), RI_{comp} is the diagnosis of the comprehensive index, RI_{cs} is the relative compressive strength value of the concrete beams calculated using Eq. (8). MATLAB is used to seek for the optimal solution of n to minimize the value of $f(n)$ and the optimum solution of n is 133 corresponding to the minimized solution of $f(n) = 0.006629$ as shown in Fig. 11. Since the objective function converges to a constant value when n exceeds 20, the coefficient n can be adopted as 20 for practical applications to reduce the calculation amount.

Aiming to illustrate advantages of the proposed comprehensive index, the results of the comprehensive index are compared to those of individual indexes as shown in Fig. 12. With the raise of volume of pellets in the concrete beams, the evaluation results are supposed to decrease gradually. However, the indexes for R-wave velocity and attenuation coefficient show opposite trend, where the R-wave velocity index (RI_2) increases from 56.96 to 58.23% with the growth of ϕ from 10 to 15%; and the attenuation coefficient index (RI_3) grows from 72.73 to 74.54% with the increase of ϕ from 10 to 15%. Thus, it can be concluded that at least one of the evaluated results of the attenuation coefficient index (or R-wave velocity index) is less reliable among the beams with $\phi = 10\%$ and $\phi = 15\%$.

The other aspect of similarity between the indexes is that the evaluation result of the R-wave velocity index $RI_2 = 56.96\%$ for Beam 3 ($\phi = 10\%$) apparently differs from the other two indexes (i.e., P-wave velocity $RI_1 = 73.91\%$ and attenuation coefficient $RI_3 = 72.73\%$), which is shown in Detail 1 of Fig. 12; while the evaluation result of the attenuation index $RI_3 = 74.54\%$ for Beam 4 ($\phi = 15\%$) is abnormal when compared to the other two indexes (i.e., P-wave velocity $RI_1 = 57.61\%$ and R-wave velocity $RI_2 = 58.23\%$) as shown in Detail 2 of Fig. 10. From this perspective, the abnormal evaluated results

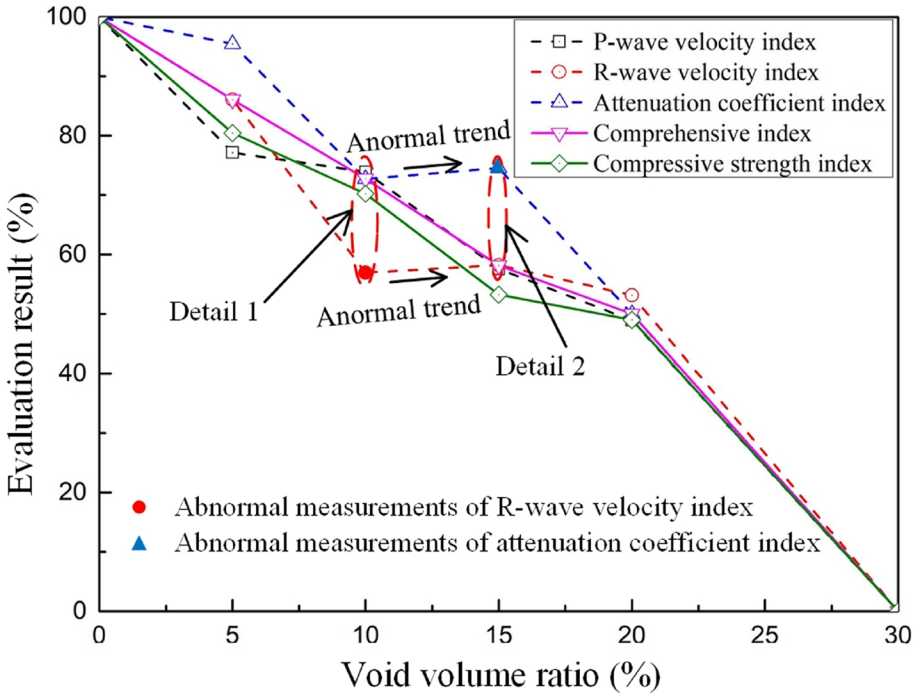

Fig. 12 Comparison of the comprehensive evaluation results with the individual evaluation ones

in this case are found to be the R-wave velocity index for Beam 3 and attenuation coefficient index for Beam 4 as highlighted in Fig. 12.

The comprehensive index can address such abnormal diagnoses as shown in Fig. 12 through lowering their weights to make them contribute less to the final evaluation result. As a result, the evaluation results of the comprehensive index in this case obey the law that the evaluation results decrease with the increase of the void volume ratio of the beams and are in good agreement with the compressive strength of the beam sections, indicating an improvement in the reliability of the assessment compared to the evaluations based on the individual indexes.

4.4 Practical application of the proposed methodology

The effectiveness of the proposed methodology is verified by using six concrete beams tested in the laboratory conditions. The reference values of C_0 and C_1 with respect to unacceptable and intact concrete condition are determined by the concrete beams with controllable void volumes. In practical applications, values of C_0 and C_1 should be defined with care according to the actual situation in situ. Moreover, the optimum solution of $n = 133$ is confined to this case study, the whole optimization process should be carried out when applied to other cases. The key point in the optimization is to determine the objective function. In the objective function, it is critical to define the baseline (i.e., compressive strength in this case study). It is suggested that some necessary destructive test need to be carried out to measure compressive strength of concrete if possible, which can be used for calibration and validation the NDT measurements.

5 Conclusions

This paper proposes a comprehensive index for condition assessment of concrete structures using the characteristics of surface waves (e.g., P- and R-wave velocities, and attenuation coefficient). The following conclusions can be drawn from this study:

(1) The characteristics of surface waves, such as P- and R-wave velocities and attenuation coefficient that are obtained from the MASW tests, can be employed as diagnostic indexes for the condition assessment of concrete structures.
(2) The selected surface wave-based characteristics for condition assessment of concrete are normalized in a relative manner due to a variety of influencing factors to the measured characteristics, either originated from the material's intrinsic properties or the test instrumentation. The relative index represents a damage scale ranging from the intact condition of material (100%) to the unacceptable condition (0%).
(3) A weighted sum method is used to aggregate the individual indexes into a comprehensive one, in which the weight of each index is determined by its credibility. The index credibility is determined based on the similarities between the individual indexes.
(4) The effectiveness of the proposed combination method for the individual diagnostic indexes is validated by using six concrete beams with different void volume ratio. The results show that the evaluation results of the comprehensive index are in good agreement with the compressive strength of the beam Sect.
(5) The proposed methodology presents a single comprehensive diagnostic feature with improved reliability on the fitness of the concrete structures for the decision-makers.

The proposed assessment method is validated by limited lab beams. More samples in the lab and field tests are needed to further validated the effectiveness of the proposed method.

Acknowledgements
The authors would like to express their gratitude for the support received.

Authors' contributions
XX carried out the molecular genetic studies, participated in the sequence alignment and drafted the manuscript. JL carried out the immunoassays. ASK participated in the sequence alignment. MAP participated in the design of the study and performed the statistical analysis. JL conceived of the study, and participated in its design and coordination and helped to draft the manuscript. All authors read and approved the final manuscript.

Funding
The research reported in this paper was supported in part by the China Scholarship Council, the National Natural Science Foundation of China under Grant No. 52308150, the Start-up Research Fund of Southeast University under Grant No. RF1028623116, the CCCC Academician Special Project under Grant No. YSZX-03-2022-01-B & YSZX-03-2021-02-B, and the grants from the Natural Sciences Engineering Research Council (NSERC).

Availability of data and materials
The datasets used and/or analysed during the current study are available from the corresponding author on reasonable request.

Declarations

Competing interests
Non-financial competing interests.

Received: 30 August 2023 Accepted: 15 October 2023
Published online: 02 December 2023

References

ASTM Committee 597 (2002) Standard test method for pulse velocity through concrete (Report No. C597-02). ASTM International, West Conshohocken

ACI Committee 228 (2003) In-place method to estimate concrete strength (Report No. ACI 228.1R-03). MI: American Concrete Institute, Farmington Hills

Belli K, Wadia-Fascetti S, Rappaport C (2008) Model based evaluation of bridge decks using ground penetrating radar. Computer Aided Civ Infrastruct Eng 23(1):3–16

Blitz J, Simpson G (1995) Ultrasonic methods of non-destructive testing. Springer Science & Business Media, New York, NY

Cheng CC, Cheng TM, Chiang CH (2008) Defect detection of concrete structures using both infrared thermography and elastic waves. Autom Constr 18(1):87–92

Cho YS (2003) Non-destructive testing of high strength concrete using spectral analysis of surface waves. NDT E Int 36(4):229–235

Goueygou M, Lafhaj Z, Soltani F (2009) Assessment of porosity of mortar using ultrasonic Rayleigh waves. NDT E Int 42(5):353–360

Graff KF (1975) Wave motion in elastic solids. Ohio State University Press, Columbus, OH

Hsieh CT, Lin Y, Lin SK (2017) Impact-echo method for the deterioration evaluation of near-surface mounted CFRP strengthening under outdoor exposure conditions. Mater Struct 50(1):72–82

Ihara I (2008) Ultrasonic sensing: fundamentals and its applications to nondestructive evaluation. Sensors 21:287–305

Karaiskos G, Deraemaeker A, Aggelis DG, Hemelrijck DV (2015) Monitoring of concrete structures using the ultrasonic pulse velocity method. Smart Mater Struct 24(11):113001

Kewalramani MA, Gupta R (2006) Concrete compressive strength prediction using ultrasonic pulse velocity through artificial neural networks. Autom Constr 15(3):374–379

Kirlangic AS (2013) Condition assessment of cemented materials using ultrasonic surface waves (Doctoral dissertation). University of Waterloo, Waterloo

Kirlangiç AS, Cascante G, Polak MA (2016) Assessment of concrete beams with irregular defects using surface waves. ACI Mater J 113(1):73–81

Lim MK, Cao H (2013) Combining multiple NDT methods to improve testing effectiveness. Constr Build Mater 38:1310–1315

Mallat SG (1989) A theory for multiresolution signal decomposition: the wavelet representation. IEEE Trans Pattern Anal Mach Intell 11(7):674–893

McCann DM, Forde MC (2001) Review of NDT methods in the assessment of concrete and masonry structures. NDT E Int 34(2):71–84

Ohtsu M (1996) The history and development of acoustic emission in concrete engineering. Mag Concr Res 48(177):321–330

Park CB, Miller RD, Xia J (1999) Multichannel analysis of surface waves. Geophysics 64(3):800–808

Popovics S (2001) Analysis of the concrete strength versus ultrasonic pulse velocity relationship. Mater Evaluation (USA) 59(2):123–124

Rodriguez Roblero MJ (2017) Condition assessment of concrete elements through two nondestructive ultrasonic techniques (Doctoral dissertation). University of Waterloo, Waterloo

Saint-Pierre F, Philibert A, Giroux B, Rivard P (2016) Concrete quality designation based on ultrasonic pulse velocity. Constr Build Mater 125:1022–1027

Sidorov G, Gelbukh A, Gomez-Adorno H, Pinto D (2014) Soft similarity and soft cosine measure: similarity of features in vector space model. Comput Y Sist 18(3):491–504

Trtnik G, Kavcic F, Turk G (2009) Prediction of concrete strength using ultrasonic pulse velocity and artificial neural networks. Ultrasonics 49(1):53–60

Yang Y, Cascante G, Polak MA (2009) Depth detection of surface-breaking cracks in concrete plates using fundamental lamb modes. NDT E Int 42(6):501–512

Zerwer A, Cascante G, Hutchinson J (2002) Parameter estimation in finite element simulations of Rayleigh waves. J Geotech Geoenviron Eng 128(3):250–261

Publisher's Note